SUPPORTING INFO file of the article

"Crystal structure and solid-state transformations of Zn-triethanolamine-acetate complexes to ZnO" published in CrystEngComm (2012) by

Eleonora Conterosito, Gianluca Croce, Luca Palin, Enrico Boccaleri, Wouter van Beek and Marco Milanesio (E-Mail to marco.milanesio@unipmn.it)

DETAILS OF SAMPLE PREPARATION

All reactants were purchased from Sigma Aldrich and used without further purification.

The most stable phase of $Zn(TEA)(Ac)_2$, namely Phase I, can be synthesized in pure form by mixing in a beaker 2-propanol (iPrOH) and TEA under stirring and then adding $Zn(Ac)_2*2H_2O$. The preparation of a mixture of $Zn(Ac)_2$ and TEA with 1:2 ratio and with $Zn(Ac)_2$ 1M in iPrOH yields a composition of 60.12 %w of iPrOH, 16.88 %w of TEA and 23.00%w of $Zn(Ac)_2$. It was found that an excess of TEA is needed for the complete conversion of $Zn(Ac)_2$. After the dissolution of $Zn(Ac)_2$, giving a clear solution, the product is formed after a few minutes of stirring as a foamy slurry. Crystallization/foaming times can be finely controlled from 3 min to 30 min decreasing the concentration of acetate from 1M to 0.1M. Large crystals (needles of about 400x40x40µm in size) of Phase I were obtained by chance, during the attempts at obtaining the hydrated form of $Zn(TEA)(Ac)_2$ complex (i.e. Phase II), by adding water to an equimolar TEA/$Zn(Ac)_2$ mixture.

$Zn_4(TEA)_2(Ac)_4$ cluster (Phase III) is obtained (after 6-7 days) with large excess of water (H_2O – acetate ratio 10:1) and acetate concentration of 0.4M. The cluster crystallized first and was found at the bottom of the beaker (i.e. formed at the end of the crystallization) while Phase II (an hydrated unstable phase) was found on the beaker surfaces. The resulting Phase II resulted pure (see section 3.1) after separation of the $Zn_4(TEA)_2(Ac)_4$ cluster by crystallization, but resulted foamy, unstable and converted in a few minutes to Phase I. Conversely, the Zn cluster (Phase III) formed large crystals, was stable and could be separated.

A further phase with a low yield can be obtained in solvent-free conditions or using less polar solvents. The XRPD pattern of this phase, named Phase IV is reported in Figure S1d. However Phase IV is impure, with wide peaks and its X-ray diffraction pattern could be neither identified nor indexed.

INSTRUMENTATION DETAILS

XRPD Data

XRPD patterns were collected using the Bragg-Brentano geometry with Cu Kα radiation (λ

=1.5418Å), and a solid-state Peltier cooled detector. All powder diffraction patterns were measured in continuous mode, using the following conditions: 2θ angular range 2-50°, tube power 45kV and 40mA; step size 0.02° 2θ. Single-crystal diffraction data were collected with an Oxford Xcalibur CCD area detector diffractometer, using graphite monochromatized Mo-Kα (λ =0.71069 E) radiation.

The Raman data were measured at room temperature by a Horiba Jobin-Yvon LabRAM HR instrument equipped with an Olympus BX41 microscope and a television camera.

TGA data were collected from 323 to 1073K in Argon with a ramp rate of 10K/min

In situ XRPD Setup

The in situ XRPD experiments were performed at the ESRF in Grenoble on the BM1B (SNBL) beamline. High resolution Powder Diffraction data were collected with the standard BM1B setup41 using a radiation with λ = 0.50038 (1)Å. The calibration was done using the lattice parameters of the NIST Lanthanum Hexaboride (LaB6) standard (SRM 660b; nominal a = 4.15695(6) Å at RT). A thermal treatment was carried out from RT to 411 K to observe and characterize the phase transitions and stability. Diffraction patterns (in the 3.5<2θ<15.5° range) were collected every 9 minutes during the thermal ramp.

First principle calculations

The Gaussian03 software was used for the first principle calculations carried out employing the DFT method. Becke's three parameter hybrid functional and Lee-Yang-Parr's gradient-corrected correlation functional (B3LYP)[1],[2] were employed, using the 6-31G(d,p) basis set[3] as implemented in the Gaussian03 software. The Raman spectra were calculated and compared to the experimental ones, after a geometry optimization of the Zn(TEA)(Ac)2 molecular complex (Figure S7).

[1] A.D. Becke, *J. Chem. Phys.*,1993, **98** , 5648-5652.

[2] C. Lee, W. Yang and R.G. Parr, *Phys. Rev. b, Condens. Matter*, 1988, **37**, 785–789.

[3] W.J. Hehre, L. Radom, P. v R. Schleyer and J.A. Pople, Ab Initio Molecular Orbital Theory. Wiley, New York, 1986.

FIGURES AND TABLES

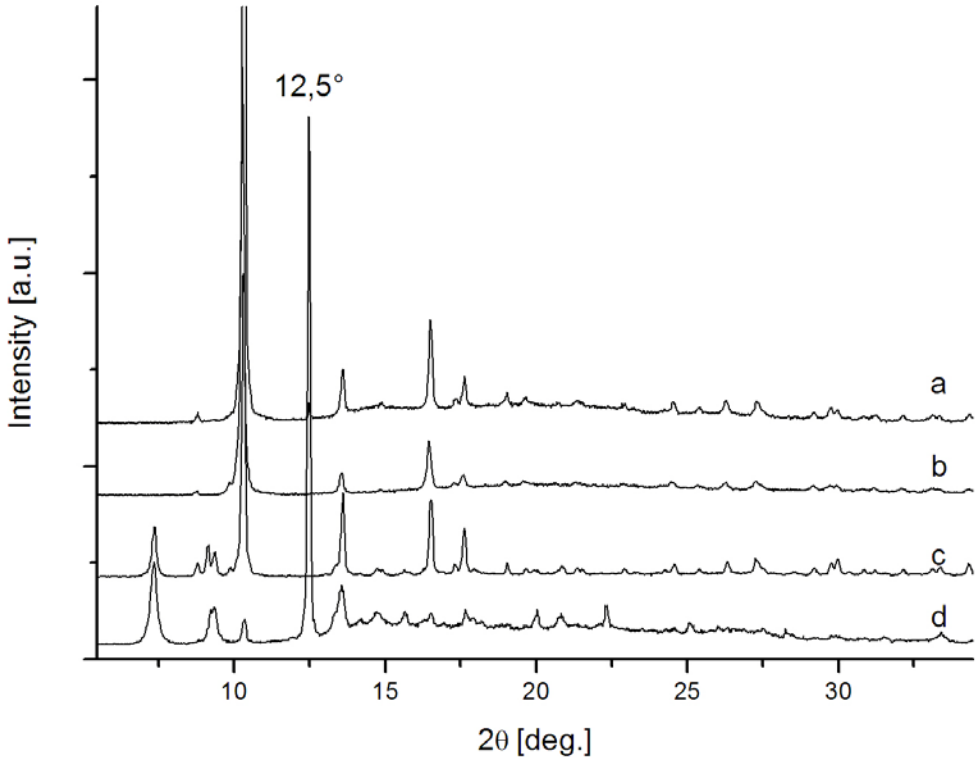

Figure S1. XRPD pattern of samples prepared using different solvents: a) 2-propanol (iPrOH) (standard synthesis as a reference) b) dimethylformammide (DMF) c) tetrahydrofuran (THF) d) without any solvent. It is possible to see noticeable differences between the patterns here reported. The profiles a) and b) of the sample, synthesized using iPrOH and DMF respectively, show the same phase. The pattern of the sample synthesized using THF leads to the formation of a different phase (Phase IV) in coexistence with Phase I . In the case of THF the reaction is complete, while without using any solvent (pattern d) the same phases are formed but we have in addiction a lot of unreacted $Zn(Ac)_2$, shown by the very intense peak at 12,5°, and just a small amount of Phase I seems to be formed.

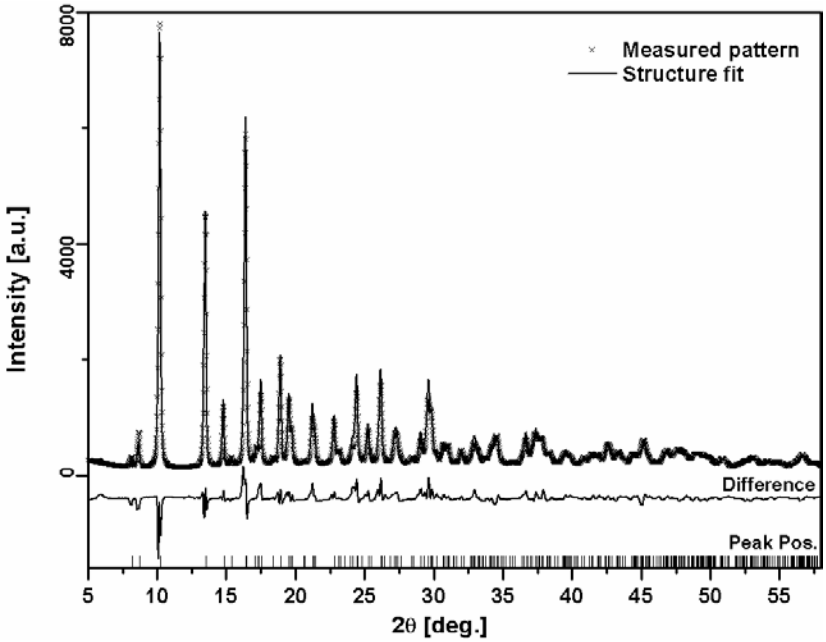

Figure S2: Fitting of the pattern calculated from the single crystal structure of $Zn(TEA)(Ac)_2$ on the XRPD pattern of the freshly prepared Phase I sample.

Figure S3 Reaction steps for the formation of the complex $Zn(TEA)(Ac)_2$: A)Mixing of the reactants (iPrOH, $Zn(Ac)_2$ and TEA). B – C) Formation of the complex after the complete dissolution of the reactants. D) Solidification (about 10 minutes after mixing the reactants).

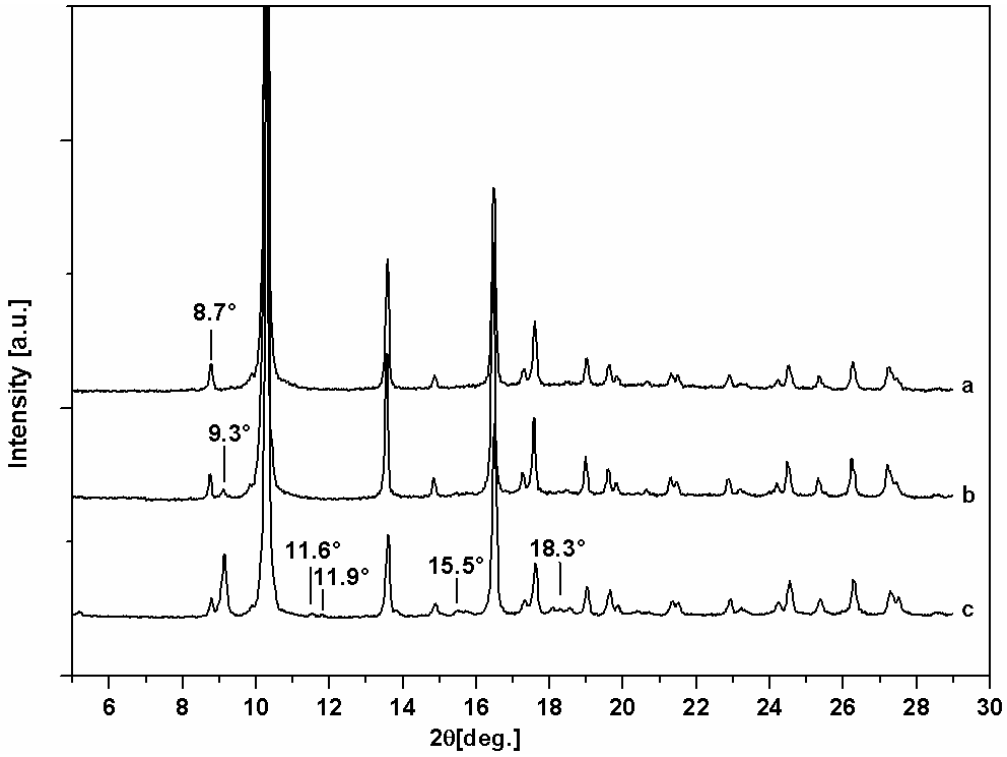

Figure S4: XRPD patterns collected after different aging times on a standard sample: a) freshly prepared sample (Phase I); b) aged 13 days; c) aged 40 days. The preliminary increase of intensity of the peak of Phase I centred at 8.7° and the subsequent decrease during aging in presence of air moisture, indicate the transformation of Phase I into a mixture of Phases I and II. After some weeks of storage two phases were present in the sample.

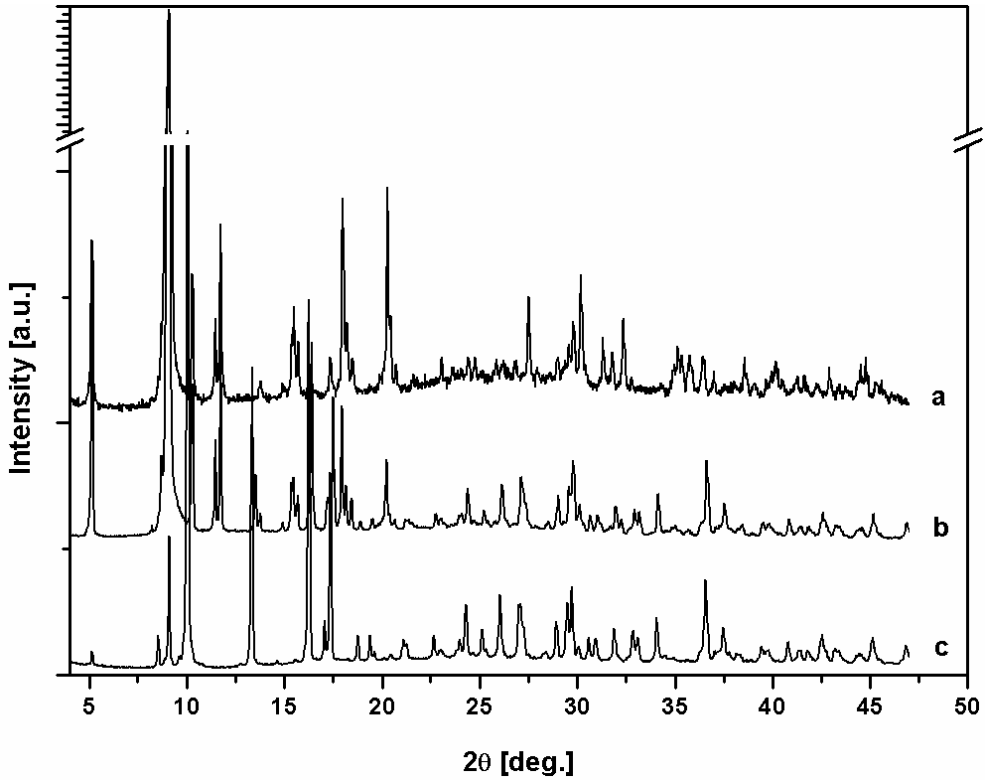

Figure S5: XRPD pattern measured on pure Phase II sample (a) showing in (b) the transition to Phase I (c) occurred during the measurement. The diffraction pattern a), collected in about 30' on the as prepared Phase II, is significantly different from that of Phase I given in c). Instead, pattern b) shows that, during the attempt at collecting a more accurate pattern of Phase II, with a smaller scan-rate, a phase transition to Phase I occurred after some time as indicated by its similarity to pattern a) up to 18-20° 2θ and its similarity to pattern c) at higher angles.

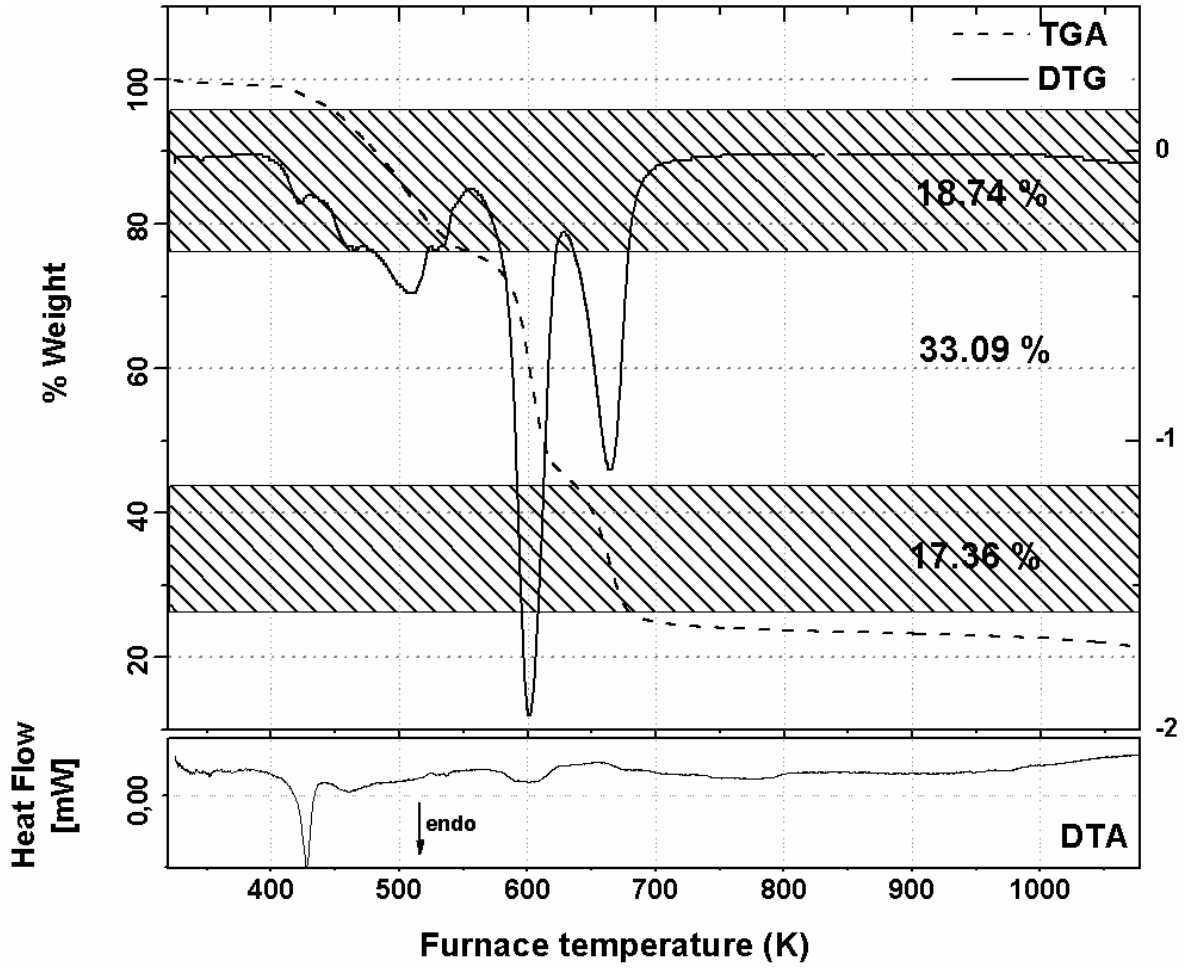

Figure S6: TGA, DTG and, at the bottom, DTA graph of Phase I sample. The thermal behaviour observed between 362 and 373 K in the XRPD synchrotron patterns (Figure 2) can be linked to the first weight loss shown between 300 and 400K in the TGA and DTA (see inset in Figure 2) of the mixed sample, while the melting is evident in the DTA and is characterized by a strong endothermic peak at ~423K. The same in situ XRPD experiment on the pure Phase I sample doesn't show any transition or structural change before decomposition.

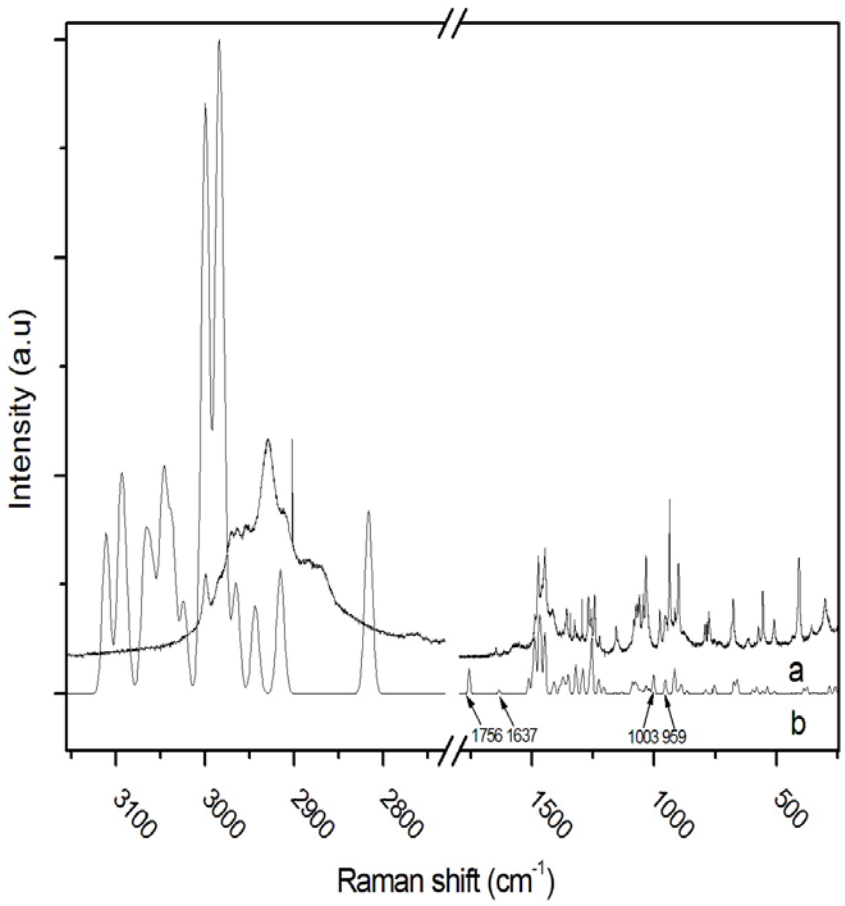

Figure S7: Calculated Raman spectrum (b) of Phase I compared with the measured one (a)

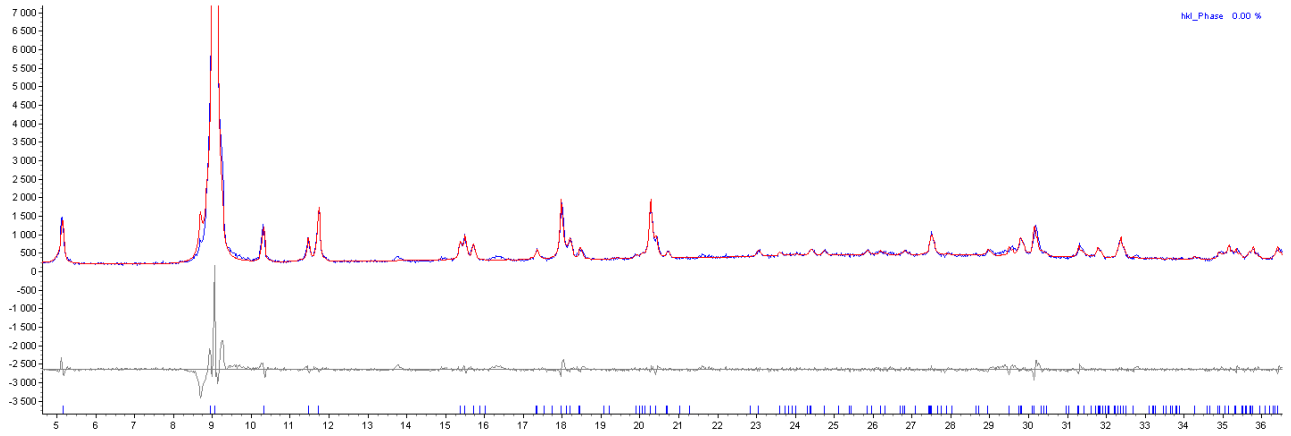

Figure S8: Indexing and Pawley fit of Phase II XRPD data (medium and low angle data).

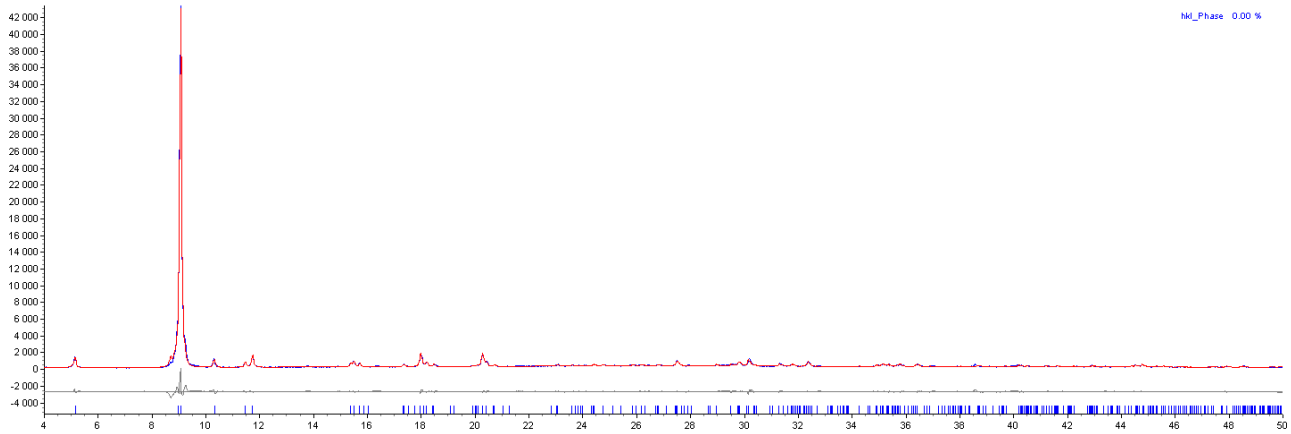

Figure S9 . Indexing and Pawley fit of Phase II XRPD data (full pattern)

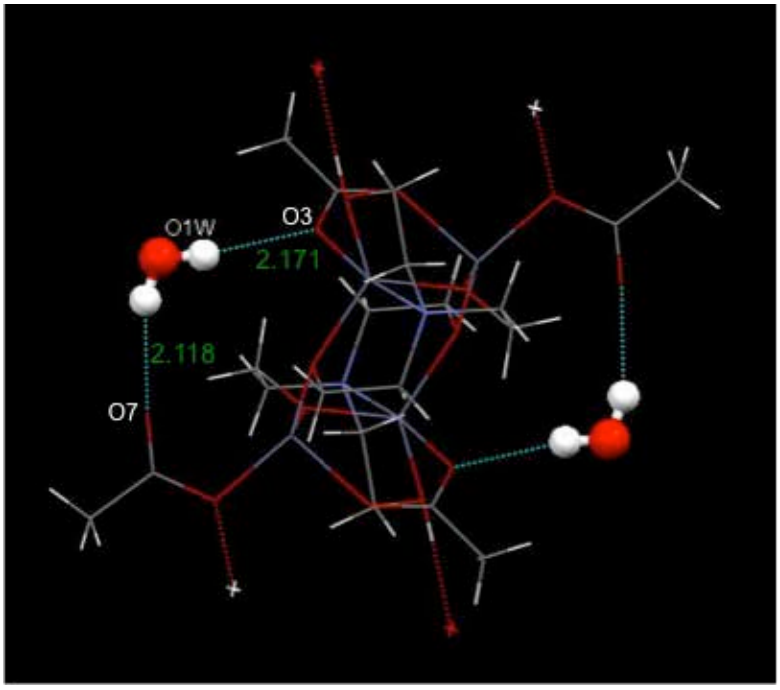

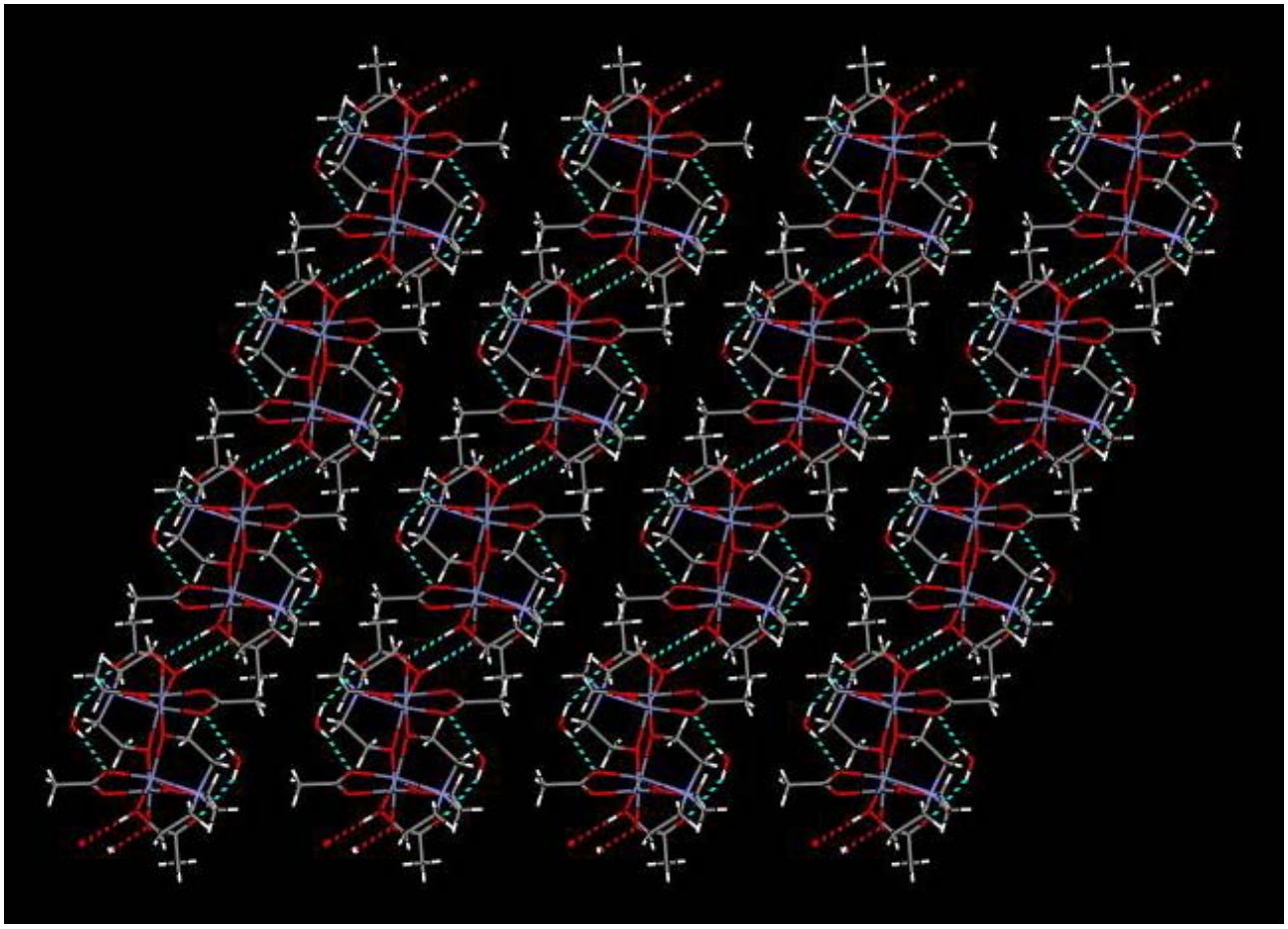

Figure S10 . H-bond features in phase III crystal structure; the images were generated by Mercury (Mercury CSD 2.0 - New Features for the Visualization and Investigation of Crystal Structures C. F. Macrae, I. J. Bruno, J. A. Chisholm, P. R. Edgington, P. McCabe, E. Pidcock, L. Rodriguez-Monge, R. Taylor, J. van de Streek and P. A. Wood, *J. Appl. Cryst.*, **2008**, 41, 466-470)

Table 1. Crystal data and structure refinement

Identification code	Phase I	Phase III
Chemical formula	$C_{10}H_{21}NO_7Zn$	$C_{20}H_{38}N_2O_{14}Zn_4 \cdot 2H_2O$
Formula weight	332.65	828.04
Wavelength	0.71073 Å	
Crystal system	Triclinic	Triclinic
Space group	P-1	P-1
Unit cell dimensions	a = 6.0895(4) Å α= 73.688(7)° b = 10.4778(9) Å β= 77.256(7)° c = 11.40869(1) Å γ □= 85.402(6)°	a = 8.4232(5) Å α = 91.118(4)° b = 10.0883(5) Å β = 113.570(5)° c = 10.1361(6) Å γ = 98.367(5)°
Volume ($Å^{3)}$	681.28(9)	778.18(9)
Temperature (K)	100	293
Z	2	1
Absorption coefficient	1.830 mm^{-1}	3.117 mm^{-1}
Density (calculated)	1.612 Mg/m^3	1.767 Mg/m^3
F(000)	344	424
Theta range for data collection	4.38 to 31.79°.	4.10 to 28.23°.
Index ranges	-9<=h<=8, -15<=k<=15, -16<=l<=16	-11<=h<=10, -12<=k<=12, -13<=l<=13
Reflections collected	22337	14250
Independent reflections	4177 [R(int) = 0.1748]	3472 [R(int) = 0.0368]
Completeness to theta = 25.00°	96.2 %	99.6%
Refinement method	Full-matrix least-squares on F^2	
Data / restraints / parameters	4177 / 0 / 172	3472 / 2 / 198
Goodness-of-fit on F^2	1.075	1.011
Final R indices [I>2sigma(I)]	R1 = 0.0962, wR2 = 0.2340	R1 = 0.0300, wR2 = 0.0624
R indices (all data)	R1 = 0.2002, wR2 = 0.2681	R1 = 0.0532, wR2 = 0.0696

Table 2: Phase I most intense peaks.

h	k	l	d_{hkl} (Å)	Rel.Intens.(%)
0	1	1	8.58113	67.43
0	1	-1	6.50473	68.11
0	1	2	5.36847	34.67
1	1	1	5.36238	65.99
0	2	0	5.02706	30.26
1	-1	1	4.65579	52.35
1	-1	-1	4.51298	34.38
1	1	-1	4.15765	32.09
1	2	0	3.8742	36.31
1	0	-2	3.62176	67.05
1	0	3	3.38526	92.62
1	3	2	3.05546	39.39
1	-2	2	2.9991	100.00
0	3	-1	2.97707	41.46
1	-3	0	2.89466	29.15
0	4	1	2.60919	28.87
2	1	-1	2.59255	33.00
2	2	0	2.5786	51.56
0	3	4	2.4387	54.74
2	0	-2	2.39506	70.89
2	-1	3	2.36308	47.32
2	3	1	2.36249	29.80
1	-3	3	2.11529	34.44
1	-3	-4	2.11055	40.36
2	4	1	2.03243	36.19

Table 3: Phase II most intense peaks.

h	k	l	d_{hkl} (Å)	Rel.Intens.(%)
0	1	1	9.74244	100.00
0	2	0	4.93293	12.94
0	1	4	4.37748	20.18
1	-2	2	3.23797	11.19
0	-1	5	2.99982	15.47
0	1	6	2.96167	27.39
0	0	6	2.85607	12.68
2	1	1	2.76458	20.53
2	0	-2	2.55116	14.05
0	4	1	2.53827	11.22
2	0	4	2.5079	8.77
0	4	0	2.46646	9.08
2	-1	4	2.33251	10.72
2	3	2	2.24912	13.38
0	-1	7	2.24089	9.35
1	3	-4	2.10532	12.52
1	3	8	2.03959	15.90
2	0	-5	2.02894	10.92
0	5	1	2.02223	24.30
2	4	5	1.89871	16.07
2	4	0	1.8741	14.21

Table 4: Phase III most intense peaks.

h	k	l	dhkl (Å)	Rel.Intens.(%)
0	0	1	9.2563	100.00
1	0	-1	7.58648	31.92
0	2	0	4.97211	31.40
1	0	-2	4.94877	36.79
0	2	1	4.23164	27.86
2	0	-1	4.16673	28.72
2	-1	-1	4.05783	67.21
2	0	0	3.80583	58.11
2	-1	0	3.77126	53.09
2	-2	0	3.30035	87.01
0	2	2	3.25158	70.43
0	3	-2	2.8113	45.85
0	3	2	2.59178	37.52
1	0	-4	2.51755	49.89
2	2	1	2.45677	65.45
1	3	-3	2.38942	29.58
1	-3	-3	2.34314	30.83
2	-4	-1	2.28527	36.12
3	2	-1	2.26113	33.10
2	-4	-2	2.17789	33.33
3	2	0	2.12088	32.31
2	-4	1	2.1185	34.61
2	2	2	2.09642	44.92
1	3	-4	2.04247	43.34
1	-1	4	2.00613	55.44
1	0	-5	1.99497	52.96
3	-4	-2	1.97514	28.92
2	-4	2	1.91217	32.70
1	-4	3	1.89405	33.24
3	-4	-3	1.86512	37.32